PB89-206643

Wind Direction Effects on Dispersion from Sources Downwind of Steep Hills

(U.S.) Environmental Sciences Research Lab.
Research Triangle Park, NC

Jan 88

U.S. Department of Commerce
National Technical Information Service
NTIS

TECHNICAL REPORT DATA
(Please read Instructions on the reverse before completing)

1. REPORT NO.	2.	3. R PB89-206643
EPA/600/J-88/335		

4. TITLE AND SUBTITLE	5. REPORT DATE
Wind Direction Effects on Dispersion from Sources Downwind of Steep Hills	January 1988 6. PERFORMING ORGANIZATION CODE
7. AUTHOR(S) I.P. Castro[1], W.H. Snyder[2] & R.E. Lawson, Jr.[2]	8. PERFORMING ORGANIZATION REPORT NO.
9. PERFORMING ORGANIZATION NAME AND ADDRESS Atmospheric Sciences Research Laboratory Office of Research and Development U.S. Environmental Protection Agency Research Triangle Park, NC 27711	10. PROGRAM ELEMENT NO. A101/B/70/09 - 3004 (FY88) 11. CONTRACT/GRANT NO. INHOUSE and Coop. Agmt. CR811973
12. SPONSORING AGENCY NAME AND ADDRESS Atmospheric Sciences Research Laboratory - RTP, NC Office of Research and Development U.S. Environmental Protection Agency Research Triangle Park, NC 27711	13. TYPE OF REPORT AND PERIOD COVERED 14. SPONSORING AGENCEY CODE EPA/600/09

15. SUPPLEMENTARY NOTES
[1]University of Surrey, Guildford, Surrey, England. [2]On assignment from the National Oceanic and Atmospheric Administration, U.S. Department of Commerce.

16. ABSTRACT

A previous experimental study of the nature of dispersion from point sources downwind of three-dimensional hills of various crosswind aspect ratio (spanwise breadth/height) has been extended to the case when the approaching wind is not normal to the spanwise axis of the hill. Surface concentration patterns resulting from sources placed at various heights have been examined, with attention limited to cases which led to the greatest concentration for the normal wind direction (θ=0). Sufficient date have been obtained to determine the terrain amplification factor (i.e., the ratio of the maximum ground-level concentration in the presence of the hill to that in its absence) for various wind directions, hills and source heights, and also to find how the ground-level concentration at the position of its maximum value for θ=0 varies with wind direction. This allows one to use wind tunnel data to estimate the effects of long-time-scale wind meander, assuming that wind-tunnel averages are equivalent to full scale averages of, say, 15 minutes.

It is demonstrated that in some circumstances the amplification factor (A) for a particular source position actually increases with small changes in wind direction. In general, however, there is a monotonic decrease in A as θ deviates from zero, which is most rapid for hills of small aspect ratio. In the case of wider hills, it is possible for the amplification factor to be reduced below unity for large θ.

17. KEY WORDS AND DOCUMENT ANALYSIS

a. DESCRIPTORS	b. IDENTIFIERS/OPEN ENDED TERMS	c. COSATI Field/Group

REPRODUCED BY
U.S. DEPARTMENT OF COMMERCE
NATIONAL TECHNICAL INFORMATION SERVICE
SPRINGFIELD, VA. 22161

18. DISTRIBUTION STATEMENT	19. SECURITY CLASS (This Report)	21. NO. OF PAGES
RELEASE TO PUBLIC	UNCLASSIFIED	12
	20. SECURITY CLASS (This page) UNCLASSIFIED	22. PRICE A01/3.95/A06.95 MF

EPA/600/J-88/335

Atmospheric Environment Vol. 22, No. 10, pp. 2229–2238, 1988.
Printed in Great Britain.

0004-6981/88 $3.00 + 0.00
Pergamon Press plc

WIND DIRECTION EFFECTS ON DISPERSION FROM SOURCES DOWNWIND OF STEEP HILLS

I. P. CASTRO
Department of Mechanical Engineering, University of Surrey, Guildford, Surrey GU2 5XH, U.K.

W. H. SNYDER* and R. E. LAWSON, JR.*
Meteorology and Assessment Division, U.S. Environmental Protection Agency, Research Triangle Park, NC 27711, U.S.A.

(*First received* 10 *June* 1987 *and received for publication* 9 *March* 1988)

Abstract—A previous experimental study of the nature of dispersion from point sources downwind of three-dimensional hills of various crosswind aspect ratio (spanwise breadth/height) has been extended to the case when the approaching wind is not normal to the spanwise axis of the hill. Surface concentration patterns resulting from sources placed at various heights have been examined, with attention limited to cases which led to the greatest concentration for the normal wind direction ($\theta = 0$). Sufficient data have been obtained to determine the terrain amplification factor (i.e. the ratio of the maximum ground-level concentration in the presence of the hill to that in its absence) for various wind directions, hills and source heights, and also to find how the ground-level concentration at the position of its maximum value for $\theta = 0$ varies with wind direction. This allows one to use wind tunnel data to estimate the effects of long-time-scale wind meander, assuming that wind-tunnel averages are equivalent to full-scale averages of, say, 15 min.

It is demonstrated that in some circumstances the amplification factor (A) for a particular source position actually increases with small changes in wind direction. In general, however, there is a monotonic decrease in A as θ deviates from zero, which is most rapid for hills of small aspect ratio. In the case of wider hills, it is possible for the amplification factor to be reduced below unity for large θ.

Key word index: Wind tunnel, topographic effects, steep hills, dispersion, directional effects.

1. INTRODUCTION

A series of experimental studies at the Fluid Modeling Facility of the U.S. Environmental Protection Agency has been undertaken during the last decade in an attempt to isolate the major phenomena governing the dispersion of scalars from point sources near hills. This work has included cases of sources placed upwind and downwind of two-dimensional low but steep ridges (Huber *et al.*, 1976; Arya *et al.*, 1981), two-dimensional hills of moderate slope (Khurshudyan *et al.*, 1981) and steep three-dimensional hills (Castro and Snyder, 1982; Snyder and Britter, 1987). In all cases, the model hills were placed with their longest axes normal to the approach flow in simulated atmospheric turbulent boundary layers. It is an obvious fact, however, that at full scale the wind direction is seldom so conveniently oriented and there is as yet virtually no quantitative information in the literature concerning the effects of changes in wind direction. Furthermore, wind meander is one of the features of the neutral atmospheric boundary layer that can lead to lateral plume widths considerably greater than might otherwise be expected (Pasquill, 1974) and may be a cause of rather lower measurements of mean plume concentration from fullscale experiments than are obtained in wind-tunnel tests.

It was specifically stated in Castro and Snyder (1982), hereafter CS, that "for axisymmetric hills, a change in wind direction is equivalent to moving the source off the centerline ($y = 0$), which will invariably lead to a reduction in the effect of the hill" and "for higher-aspect-ratio hills, the opposite trend may occur". These remarks to some extent beg the question, but there is no doubt that, as was also stated, "further work is necessary to quantify the effects". In our earlier work with sources downstream of various hills (CS), it was shown that the overall wake dynamics were not strongly dependent on the hill aspect ratio, α. While for the conical hill it was possible to discern the effect of axial vorticity on the dispersion process, this was not particularly dominant. The diffusion processes occurring not too far downstream of reattachment were found to scale, for practical purposes, on x_R, the distance to reattachment (i.e. the length of the 'hill plus its cavity zone'), so that for sources located at $x_s = cx_R$ ($c > 1$), the centerline surface concentration was largely independent of hill aspect ratio. Now it is not clear whether this would remain the case for wind directions not normal to the longer axis of the hill. Intuitively, it would perhaps be expected that the spanwise mean flow in the wake, induced by the asymmetry, and the generation of an asymmetric axial vorticity field would lead to rather different behavior for hills of

* On assignment from the National Oceanic and Atmospheric Administration, U.S. Department of Commerce.

NTIS is authorized to reproduce and sell this report. Permission for further reproduction must be obtained from the copyright owner.

different aspect ratio. For an axisymmetric hill, of course, these asymmetries in the flow do not occur at all, whereas for a very wide hill they must be quite strong.

A very extensive program of work would be required to study these points in detail and it would clearly be necessary to investigate the flow field as well as the concentration field. While such an investigation would not be without interest, from a practical point of view it seemed more important simply to find the major effects of wind direction on the location and magnitude of the maximum surface concentration. That is the purpose of the present work.

We have not studied wind direction effects for cases with the source upstream of the hill. Snyder and Britter (1987) have shown that terrain amplification factors do not in that case exceed about four (for axisymmetric hills) and for wider hills are usually much lower. By contrast, for sources downwind, Fig. 1 (taken from CS) shows that peak A-values range between about 6 and 7.5 for source heights equal to the hill height ($H_s/h=1$), if the source is located near the end of the separated region, i.e. at $x_s/x_R=1$, where x_R is the distance from the center of the hill to the point of mean-flow reattachment. (Throughout this paper, A is defined as the terrain amplification factor—the ratio of the maximum ground-level concentration in the presence of the hill to that in its absence. Note that the maxima in the presence and in the absence of the hill will almost certainly occur at different positions relative to the source; the terrain amplification factor is a ratio of these maxima and is a function of source position only.) In the single case of a two-dimensional hill, A could exceed 10 for $x_s/x_R=0.5$ (not shown). The hills had triangular side elevations with slopes of 1 in 2 and were therefore steep enough to ensure separation at or near the peak. Even for hills of sufficiently small slope to avoid separation, A can still exceed 10 for downwind sources (Khurshudyan *et al.*, 1981), so from a practical viewpoint these are usually the most serious cases.

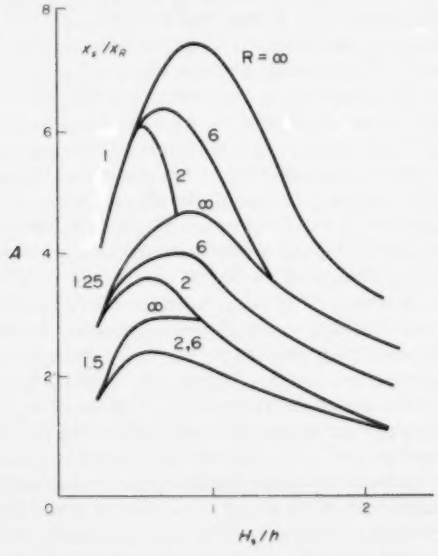

Fig. 1. Variation of terrain amplification factor for sources at or downwind of the reattachment point. ($R = L/h$, nominal hill spanwise aspect ratio; see Fig. 2.) From Castro and Snyder (1982). Wind direction is normal to hill in all cases.

In the present work, two major objectives were in view: the first was to determine how the amplification factors for various hills and source positions varied with wind direction. In view of the enormous quantity of data required for a fully comprehensive study of this kind, covering a wide range of source locations, hill shapes and wind directions, it was decided to concentrate attention on the particular cases that generally led to the highest amplification factors in the case when the wind was normal to the hill. From a practical and regulatory point of view, this is often the 'worst' condition, and, as indicated above, it usually occurred for sources located at an axial station close to the end of the separated region in the lee of the hill. The second objective was to determine how the ground-level concentration (glc) at the position of its maximum for zero wind direction varied with wind direction. Coupled with statistics of wind meander in the full-scale situation, this could eventually lead to estimates of the effect of such meander on the glc at this 'worst' position. Note that the source was placed at a fixed position on the lee side of the hill and that the hill and source were rotated as a unit in order to vary the wind direction.

We have also limited the study to just two hills: the conical hill and the widest of the three-dimensional hills used in CS. The wider three-dimensional hill is probably more typical of wide hills at full scale than is a fully two-dimensional one.

2. EXPERIMENTAL DETAILS

All the experimental work was undertaken in the EPA Fluid Modeling Facility's open-return Meteorological Wind Tunnel, which has a working section 3.7 m wide, 2.1 m high and 18.3 m long. A neutrally stable atmospheric boundary layer was simulated using a 153-mm-high fence mounted 650 mm downstream of the contraction exit and followed by gravel roughness, with dimensions up to about 10 mm, covering the entire floor of the working section. The boundary-layer thickness, δ, was about 800 mm at the location where the hills were mounted—nominally 8.5 m from the fence. Its characteristics are described in CS, where it is shown that the flow is representative of a 'moderately rough rural type' of atmospheric boundary layer (Counihan, 1975), having an equivalent surface roughness length of about 100 mm. Measurements of plume growth rates indicated that the diffusive characteristics of the boundary layer were similar to those of Pasquill–Gifford stability class C–D (Turner, 1970) which is typical of boundary layers developed in this way (Robins, 1978).

The two hills were the same ones as those used by CS. They had a nominal height of 245 mm, so that $h/\delta=0.3$. The base diameter of the cone (C2) was $4h$ and the wider hill (C6) was obtained by inserting a straight-sided triangular section of

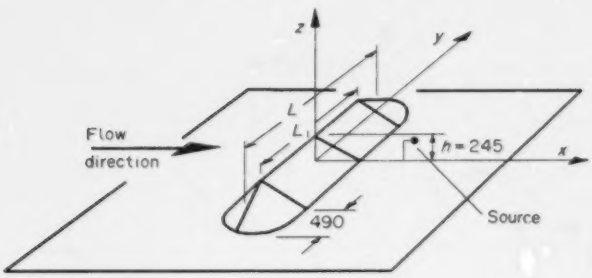

Hill	C2	C6
L_1 (mm)	0	900
L (mm)	460	1360
L/h	2.0	5.8

Fig. 2. Experimental arrangements. Dimensions in mm. Not to scale.

length $4h$ and width $3.7h$ between the two halves of the basic cone. In both cases the ceiling height was adjusted to ensure zero longitudinal pressure gradient in the free stream. Figure 2 shows the general arrangement.

For the concentration measurements ethylene (C_2H_4) and, later, ethane (C_2H_6) was used as a tracer gas. In the first stages of the work the tracer was emitted from a sintered bronze ball of 15 mm diameter at the end of a stack with a 90° bend, using a volume flow rate Q of about 5000 cm^3 min^{-1} with a free-stream velocity U_r of about 8 m s^{-1}. For the later ethane measurements a rather smaller perforated hollow plastic ball was used as the effluent source with $Q = 3000$ cm^3 min^{-1} and $U_r = 4$ m s^{-1}. These changes led to noticeable differences in measured concentrations (normalized as below), with the later data generally lying slightly below the earlier results. However, with the concentration spanning several decades in any typical profile, these differences, which were generally no greater than about 10%, were relatively insignificant. Indeed, since the measurements were obtained at varying times over a period of 4 yr, the differences were encouragingly small.

In all cases Q was monitored using a calibrated Meriam laminar-flow element and a micromanometer. Concentration profiles were obtained by collecting up to four simultaneous samples through rakes of 1.6-mm o.d. tubes which could be traversed in all three directions. These samples were passed through Beckman hydrocarbon analyzers, with the outputs digitized at a rate of 10 Hz and averaged on-line either by a PDP 11/40 minicomputer or an IBM PC/XT-compatible microcomputer. Linearity checks of the flame ionization detectors were performed regularly with 'zero', 'span' and 'background' measurements being taken frequently—the last at least twice during every individual profile to allow correction for the non-zero tracer background level in the laboratory.

The software normalized the corrected concentration (C', parts ethylene or ethane per part air by volume) by

$$C = C' U_r h^2 / Q.$$

h was taken as 245 mm throughout. Two-min averages were generally used; in the later stages with $U_r = 4$ m s^{-1}, this led to a little more scatter than in the earlier work, but this was still acceptably low. Figure 3 shows surface concentration profiles downwind of stacks of heights $H_s/h = 0.25$, 0.5, 0.75, 1, 1.5 and 2 in the absence of any hill. These were obtained in the later stages of the work and therefore may differ very slightly from those shown in CS, for the reasons outlined above, and provided the 'baseline' values of the maximum surface concentration C^*_{max} used to estimate terrain amplification factors.

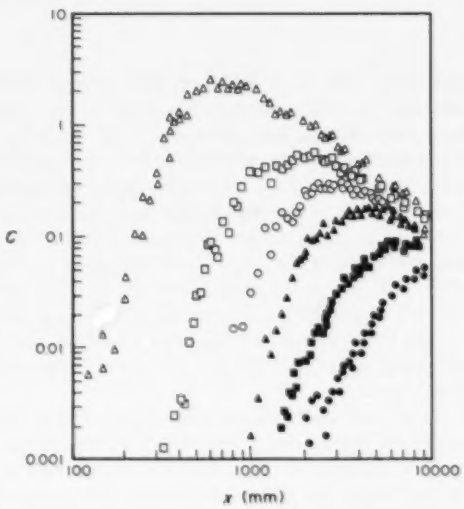

Fig. 3. Surface concentration profiles downwind of point sources in flat terrain. x is distance from source. H_s (mm), H_s/h (nominal): △, 59, 0.25; □, 117, 0.5; ○, 176, 0.75; ▲, 234, 1.0; ■, 351, 1.5; ●, 468, 2.0.

3. RESULTS

Notation

To assist in the presentation and discussion of the results, Fig. 4 defines the notation used. S denotes the location (x_s, y_s) of the source, which was fixed at 600 or 1300 mm from the hill center ($x = y = 0$) for C2 or C6, respectively, coinciding with x_R, the mean reattach-

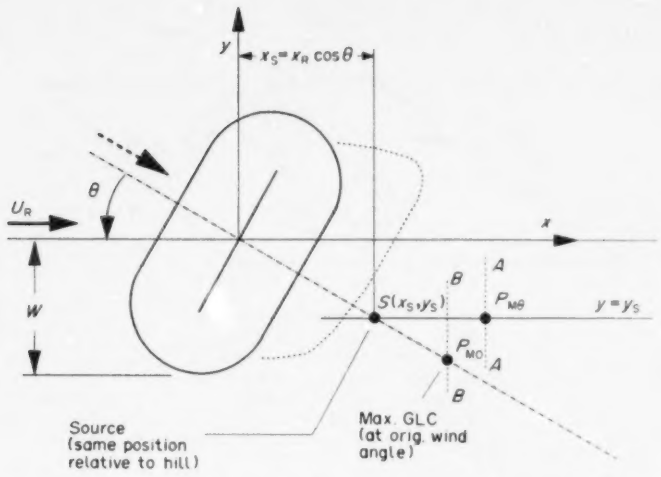

Fig. 4. Notation. $x_R = 600$ mm (C2) or 1300 mm (C6). Traverses made along $y = 0$ (for C2 only), $y = y_s$, A–A and B–B.

ment point (on $y = 0$) for $\theta = 0$. For various wind directions up to 45°, surface concentration traverses were made along a line downwind of $S(y = y_s)$ and, occasionally, along the line passing through the origin and S. In addition, for C2, traverses along $y = 0$ were made since for this axisymmetric case this can be thought of as giving the changes in the concentration field arising from different lateral locations of the source. Effectively the source is swept through the wake of the hill along a circular arc of radius x_R. For C6, interpretation of such traverses would be much less simple so that data along $y = 0$ were not obtained in that case.

For any particular source height, P_{M0} denotes the location of the maximum concentration that occurs for $\theta = 0$, obtained in the earlier study (CS), and $P_{M\theta}$ the location of the maximum concentration along $y = y_s$. CS showed that C_{gmx}, the maximum surface concentration anywhere, does occur on the symmetry line ($y = 0$) for $\theta = 0$, but there is no reason to suppose that for $\theta \neq 0$, C_{gmx} will occur on $y = y_s$. Lateral surface traverses were therefore obtained along a line through $P_{M\theta}$ (the line A–A). These often showed that the concentration at $P_{M\theta}$ was not, in fact, the maximum, but further checks confirmed that C_{gmx} was always close to the lateral line through P_{M0}. Additional more restricted lateral traverses were made through P_{M0} (the line B–B) so that the effect of wind direction on the concentration there could be assessed.

Whereas a large volume of data was collected, including axial and lateral profiles for numerous stack heights and numerous wind directions, only a small portion of the 'raw data' plots are presented herein (section 3) to provide some samples and to show general trends. The full data set is used for the 'deduced results' presented in section 4.

Data for axisymmetric hill, C2

Typical longitudinal profiles along $y = y_s$ for $\theta = 0$, 7.5, 15, 22.5, 30 and 45° are shown in Fig. 5. Figure 5a refers to a source height of 0.25 hill heights, and Fig. 5b to a source height of one hill height. Results for the no-hill, flat-surface data (Fig. 3) are included for comparison. On each plot the abscissa is x, the distance from the hill centerline (Fig. 4), so note that the source location is different for each wind angle ($x_s = 600 \cos\theta$) and that the no-hill profiles have been plotted as C vs 'the distance from the source plus 424 mm' for ease of comparison with the $\theta = 45°$ results.

For large enough θ and low enough H_s, it was anticipated that the surface concentration profiles would collapse to the no-hill case. Clearly $\theta = 45°$ and $H_s/h = 0.25$ are sufficiently large and small, respectively, for the data to be practically indistinguishable from the flat-surface results, despite the fact that the source is still slightly nearer $y = 0$ than is the extreme base of the hill. However, as H_s/h rises the differences between the no-hill results and the $\theta = 45°$ data increase (Fig. 5b). In these cases the surface concentration is higher everywhere along $y = y_s$ than it is over the flat surface, probably as a result of the combined effects of the downwash caused by axial vorticity (CS) and the increased turbulence in the wake. (Note that this trend would not be expected to continue indefinitely as H_s/h increases, but $H_s/h \gg 1$ is not a case of practical interest.) For large enough θ, the effective lateral source location would be outboard of the trailing axial vortex centerline, leading to upwash of the plume. This would counteract the effect of increased vertical turbulence, but in the absence of data for $\theta > 45°$, it is not clear whether it would be sufficient to lead to reductions in surface concentration. For less

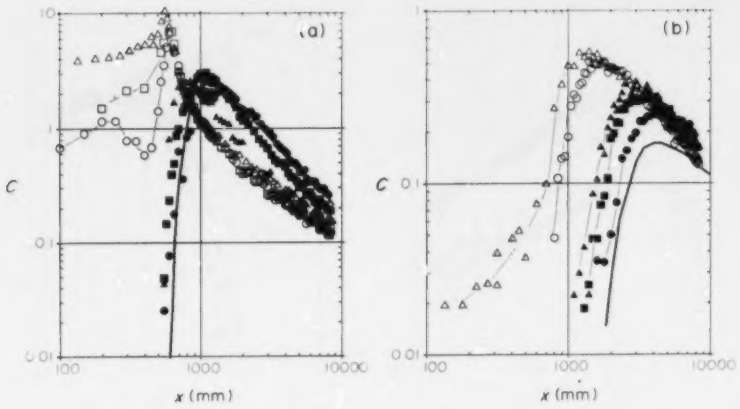

Fig. 5. Surface concentration profiles along $y = y_s$. Hill C2. θ: △, 0°; □, 7.5°; ○, 15°; ▲, 22.5°; ■, 30°; ●, 45°. (a) $H_s/h = 0.25$; (b) $H_s/h = 1.0$. Heavy solid lines are for flat terrain with abscissa of $(x - x_s) + x_R \cos 45°$.

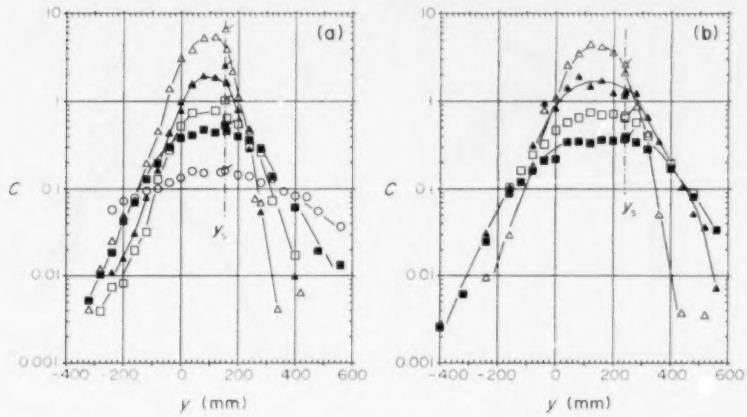

Fig. 6. Lateral concentration profiles through $P_{M\theta}$ (along A–A, Fig. 4). Hill C2. H_s/h: △, 0.25; ▲, 0.5; □, 0.75; ■, 1.0; ○, 1.5. Dashed symbols are from axial profiles along $y = y_s$. (a) $\theta = 15°$, $y_s = 155$ mm; (b) $\theta = 22.5°$, $y_s = 240$ mm.

extreme wind directions the profiles show increasingly early locations of the peak concentration, which is invariably larger than the flat-surface value but always smaller than the $\theta = 0$ result.

Figure 6 shows typical lateral concentration profiles through $P_{M\theta}$, with the values of C at $P_{M\theta}(y = y_s)$ deduced from smooth lines through the axial profiles included. The latter confirm the general consistency of the measurements except in two or three instances; in these cases the profiles were scaled to match the $C_{M\theta}$ value from the corresponding axial traverse for all later data manipulations. For $\theta = 15°$ (Fig. 6a) and 45° (not shown), the location of C_{gmx} is very close to $P_{M\theta}$, but for intermediate wind angles, particularly 22.5° (Fig. 6b), its magnitude is significantly greater than the concentration at $P_{M\theta}(C_{M\theta}$, say). In the intermediate cases, the location of C_{gmx} is always closer to $y = 0$, which must be a result either of the axial vorticity generated by the hill or the tendency of the mean streamlines to converge towards $y = 0$ beyond the separated wake region.

Results of the raw axial profiles along $y = 0$, which have a similar form to those along $y = y_s$, and the short lateral profiles through P_{M0} will not be presented in detail. Discussion of their more important features is included in section 4.

Data for the wider hill, C6

Longitudinal profiles along $y = y_s$ for $\theta = 0$, 5, 10, 15, 30 and 45° are shown in Fig. 7. Figure 7a refers to a source height of 0.25 hill heights and Fig. 7b to a source height of 1.0 hill heights; results from Fig. 3 for

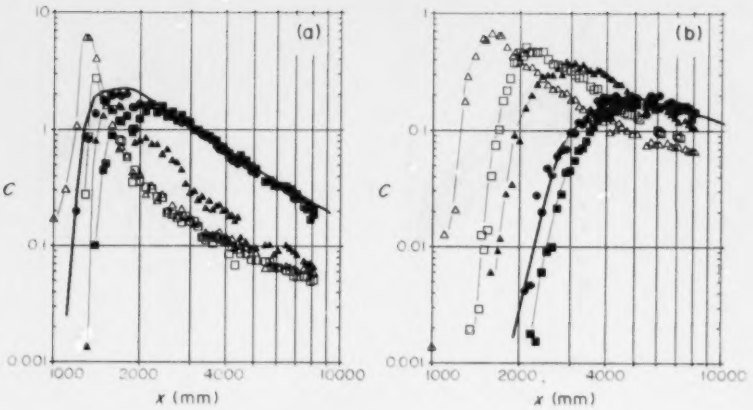

Fig. 7. Surface concentration profiles along $y = y_s$. Hill C6. θ: △, 0°; □, 10°; ▲, 15°; ■, 30°; ●, 45°. (a) $H_s/h = 0.25$; (b) $H_s/h = 1.0$. Heavy solid lines are for flat terrain with abscissa of $(x - x_s) + x_R \cos 45°$.

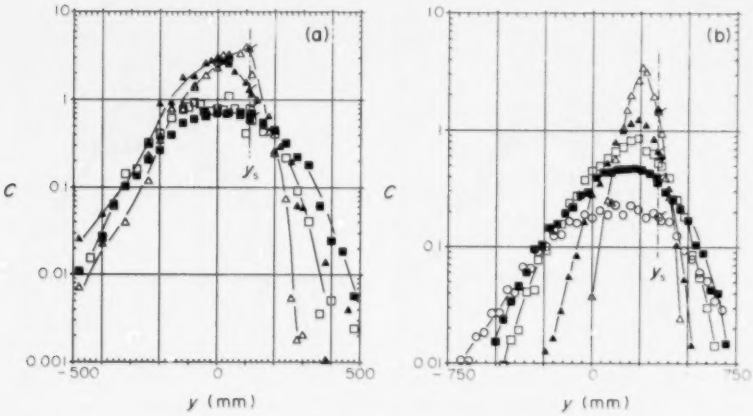

Fig. 8. Lateral concentration profiles through $P_{M\theta}$ (along A–A, Fig. 4). Hill C6. Symbols as in Fig. 6. (a) $\theta = 5°$, $y_s = 113$ mm; (b) $\theta = 15°$, $y_s = 336$ mm.

the no-hill data are also included. In the latter case the abscissa is 'distance from the source + 920 mm', for comparison with the $\theta = 45°$ results. Although the peak value of the $\theta = 45°$ data is about 10% lower than the flat-surface data, reasonable collapse is again seen for $H_s/h = 0.25$ (Fig. 7a). From Fig. 7b, we may surmise that rather greater source heights are required before differences become significant than were necessary in the case of the axisymmetric hill. This can be explained by the fact that, for a given wind angle, the source is relatively farther away from $y = 0$ for the C6 hill than it is for C2; at $\theta = 45°$, for example, $x_s \cos\theta$ (920 mm) is actually farther from $y = 0$ than is the spanwise edge of the C6 hill—for C2 hill it is nearer, as noted earlier. To quantify these differences in source location, it is helpful to define W as the base half-width of the hill at any angle—see Fig. 4. For C6, $W = (490 + 450 \cos\theta)$ mm and for C2, $W = 490$ mm. Hence, at $\theta = 45°$, y_s/W is 1.14 for C6 but only 0.94 for C2; the corresponding figures at $\theta = 5°$ are 0.121 and 0.106.

Figure 8 shows some lateral concentration profiles through $P_{M\theta}$, with $C_{M\theta}$ values from the axial profiles again included. In these cases, even for $\theta = 5°$, the location of $C_{\theta max}$ is closer to $y = 0$ than is y_s and the magnitudes are, in some cases, factors of two greater than $C_{M\theta}$.

4. DEDUCED RESULTS AND FURTHER DISCUSSION

We start by considering the effect of the wind direction on the terrain amplification factor A. Figure 9 shows A as a function of H_s/h for constant wind angles. The general form of the earlier CS results for $\theta = 0$ is maintained at all θ for both hills, with the maximum amplification factors occurring for source

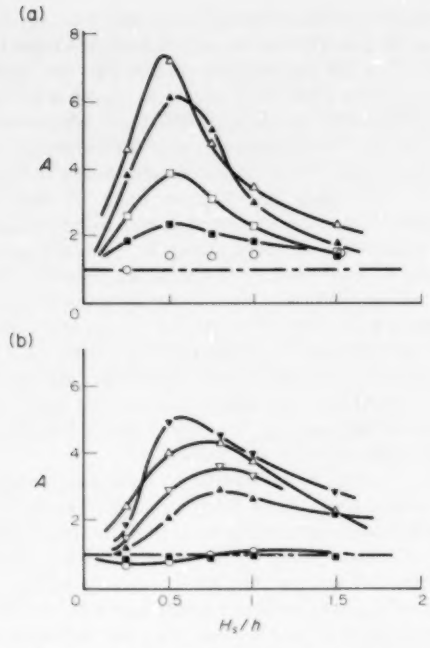

Fig. 9. Terrain amplification factor. θ: ▵, 0°; ▾, 5°; ▿, 10°; ▲, 15°; □, 22.5°; ■, 30°; ○, 45°. (a) C2; (b) C6.

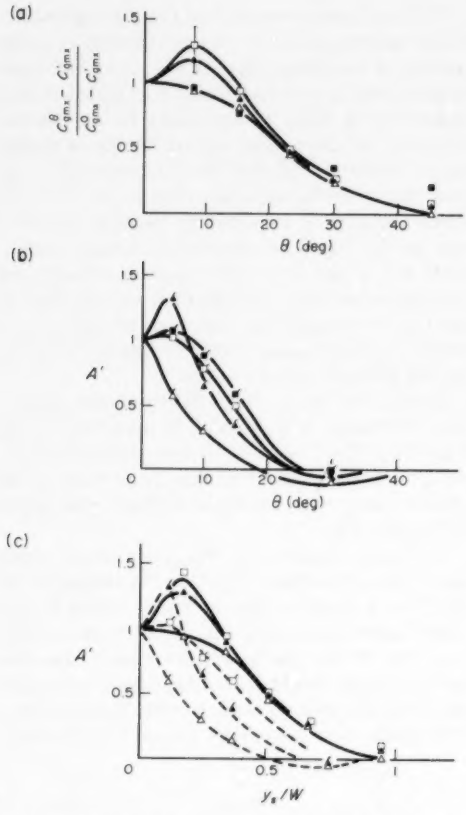

Fig. 10. Variation of $A' = (C^{\theta}_{gmx} - C^{\infty}_{gmx})/(C^{0}_{gmx} - C^{\infty}_{gmx})$ with θ for: (a) C2; (b) C6; (c) variation with y_s/W for C2 and C6. H_s/h: ▵, 0.25; ▲, 0.5; □, 0.75; ■, 1.0. Dashed symbols (and broken lines) are for C6. Lines added for clarity.

heights between 1/2 and 3/4 of the hill height; there is a slight tendency for the source height yielding maximum A to increase with wind angle, especially for C6. In the particular case of the wider hill (Fig. 9b) and $\theta = 5°$, the maximum A is actually larger than at $\theta = 0°$. Now, for small H_s, the value of C_{gmx} must be largely determined by the local turbulence field, whereas for taller stacks the influence of swirling motions will be more significant; for large enough wind angles, the hill will not affect the near-field turbulence downwind of the source, whereas farther downstream, the remaining mean axial vorticity may tend to pull the plume towards the surface.

Despite this broad feature of the results, it is evident from Fig. 9 that the trend in A with θ is not always monotonic. This is emphasized in Fig. 10, where $(C^{\theta}_{gmx} - C^{\infty}_{gmx})/(C^{0}_{gmx} - C^{\infty}_{gmx})$ is plotted against θ. Here C^{∞}_{gmx} and C^{0}_{gmx} are the maximum ground-level concentrations (glcs) over flat terrain and in the presence of the hill with $\theta = 0$, respectively. This function was chosen because it must tend to zero as $\theta \to 90°$ (provided x_R is large), unlike the ratio of the amplification factors for θ and $\theta = 0$. For $H_s/h = 0.5$ (and 0.75 for C2), there is a distinct rise in peak concentration for small non-zero wind angles before the inevitable fall to flat-surface values at large θ. Lateral turbulence energy profiles often show distinct peaks on each side of $y = 0$, corresponding to the location of the shear layers shed from the obstacle (CS), and it is possible that at these source heights and y_s values, the plume is injected directly into this high-turbulence region, leading to increased vertical dispersion and, hence, larger glcs.

As a more meaningful comparison of the behavior for the two different hills, the data for stack heights between 0.25 and 0.75 are replotted against y_s/W in Fig. 10c (recall that W is the distance between $y = 0$ and the extreme spanwise edge of the hill; see Fig. 4). The peak glcs are generally much higher at a given y_s/W in the case of the axisymmetric hill than they are for the wider hill. Now in CS it was shown that the mean axial vorticity generated by C2 is relatively persistent, leading to a significantly reduced decay of glc in the far field for $\theta = 0$ compared to that behind wider, or even two-dimensional, hills. It would seem that this mean vorticity is also more effective in maintaining high amplifications at non-zero wind angles than are the greater turbulence perturbations generated by the wider hill.

Two other features should be noted. First, for the wider hill, there is a clear hint of reductions (amplification factors < 1) in peak glcs for y_s/W around 0.75 (θ

$= 30°$) for all source heights. This could be the result of plume upwash caused by its location relative to the position of the strong single axial vortex which must be generated by this asymmetric configuration. It is perhaps more likely to be caused by an effective movement of the source relative to the separated region behind the hill. For this wind angle (30°), the axial extent of the separated region at $y = y_s$ will almost certainly be considerably less than x_r, and it may be that enhanced spanwise turbulence components and a non-zero mean spanwise velocity are sufficient to increase plume dispersion at elevation. In any case, it is interesting that, even at these source locations, which are well within the spanwise extent of the hill, the peak glcs are so low.

Second, the results for different source heights largely converge in the case of the axisymmetric hill (Fig. 10a), at least for $\theta > 10°$, whereas they clearly do not for the wider hill. This may be a result of the different levels of asymmetry at different wind angles in the latter case.

In all cases except $\theta = 45°$, the maximum glc occurs nearer the source than it would in the absence of the hill. This is demonstrated in Fig. 11 where $C_{M\theta}$ is plotted against downwind distance from the source ($x - x_s$). For $\theta = 45°$ the results are close to the flat-surface data for both hills, but the data at all smaller wind angles lie monotonically between these and the $\theta = 0°$ results. Note that on this plot, as H_s/h decreases for fixed θ, the data have higher $C_{M\theta}$ and lower $(x - x_s)$, as usual. The trend is similar but much less rapid for fixed H_s/h and decreasing θ; dashed lines are drawn through the fixed H_s/h points in the case of C2 (Fig. 11a). These should not, of course, be extrapolated beyond the $\theta = 0$ data points—symmetry requires that results at, say, $\theta = 10°$ should be coincident with those at $\theta = -10°$. Note also that the wider hill leads to significantly earlier locations of the maximum glc, particularly for tall sources (large H_s/h, small $C_{M\theta}$), as would be anticipated. It is interesting, however, that the one set of C2 data ($\theta = 15°$) having a similar y_s/W value to a C6 set ($y_s/W = 0.35, \theta = 15°$) collapses quite well with the latter when plotted in this form; Fig. 11b includes these C2 data, but it should be emphasized that, except for the tallest sources, the $C_{M\theta}$ and corresponding $(x - x_s)$ for a given source height are quite different in the two cases.

These trends are rather different from those found in an earlier study using much smoother two-dimensional hills (Khurshudyan *et al.*, 1981). In those cases, for all sources except those just downstream of the steepest hill and therefore within a separated region, C_{mx} vs x_{mx} data collapsed rather well with the flat-terrain data. It would seem that the influence of relatively large separation regions and, possibly, significant three-dimensionality (e.g. axial vorticity) must be the causes of this difference.

A further rather remarkable feature of the results is demonstrated in Fig. 12. Here some of the lateral surface concentration profiles are plotted in non-dimensional form, using $\bar{y}$ and σ_y, the mean and standard deviation of the profile, and C_{gmx}, the maximum glc, in each particular case, as normalizing

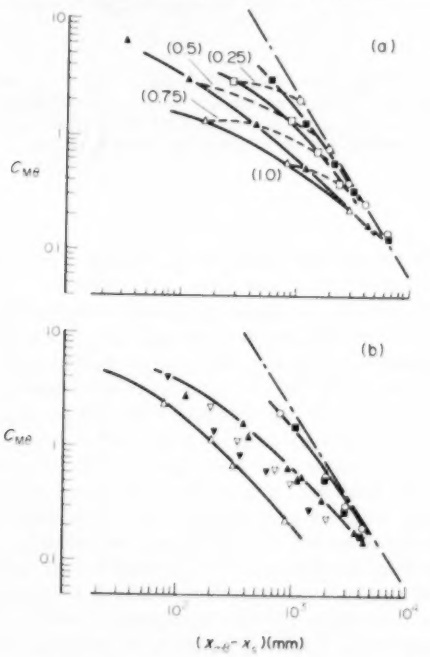

Fig. 11. Concentration at $P_{M\theta}$ vs distance of $P_{M\theta}$ from source. θ: △, 0°; ▼, 5°; ▽, 10°; ▲, 15°; □, 22.5; ■, 30°; ○, 45°. (a) C2. Dashed lines join fixed H_s/h points with values shown in brackets. (b) C6 (▲, C2 data). — — — —, flat terrain data.

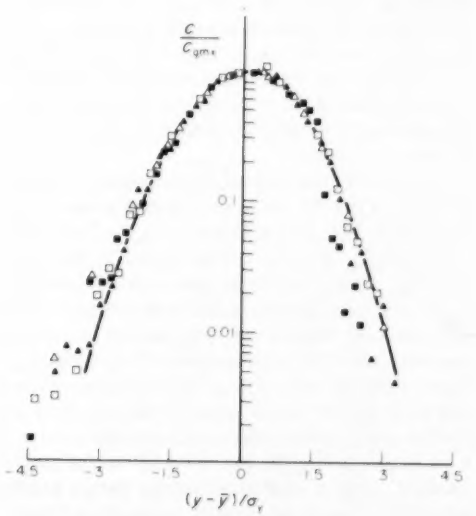

Fig. 12. Normalized lateral concentration profiles. Hill C6, $\theta = 30°$. H_s/h: △, 0.25; ▲, 0.5; □, 0.75; ■, 1.0. ——, Gaussian curve.

parameters. Despite the asymmetric nature of the flow field for non-zero wind angles, the profiles are surprisingly close to the standard Gaussian profile which occurs in flat terrain. This is true even for the wide hill and relatively large wind angles. Figure 12 shows the data for C6 and $\theta = 30°$; profiles in less extreme cases are even closer to Gaussian. Only in the extreme tails of the distributions, which are emphasized by the log–linear nature of the plot, can the slight skewness of the profiles be clearly seen. In all cases rather higher glcs are apparent on the 'inside' of the distribution (i.e. nearer the $y = 0$ line), as might have been anticipated. Although only a few profiles are shown, they are typical of all those obtained and emphasize that extremely strong flow asymmetries would be required before highly non-Gaussian lateral surface profiles would be expected downwind of sources of any height.

Finally, from the few lateral traverses through P_{M0} (not presented), it was possible to deduce how the concentration at this fixed location (where the glc is a maximum for $\theta = 0$) varied with θ. The results are shown in Fig. 13, where C^{θ}_{M0}, the value of the glc at C_{M0} for a wind angle θ, has been normalized by its value at $\theta = 0$. Few data points are available, but plausible lines are drawn through them and it seems clear that the fall in concentration at this point is much more rapid for the taller stacks. This was anticipated, since x_{M0} increases rapidly with H_s/h, but it should be noted particularly that even for short stacks the glc drops to nearly zero when θ exceeds about 20°.

Long-term wind meander—changes in wind direction on time-scales longer than those associated with the usual boundary layer turbulence—could therefore lead to substantial reductions in concentration at this 'worst' position for $\theta = 0$. An estimate of the magnitude of this effect can be obtained as follows. With $p(\theta)$ defined as the probability density distribution of the wind-meander and $C^{\theta}_{M0}/C^{0}_{M0}$ represented by $C_r(\theta)$, then the mean value of $C_r(\theta)$ is given by

$$C_{rm} = \int_0^{2\pi} C_r(\theta) p(\theta)\, \mathrm{d}\theta.$$

As an example, a simple representation of $C_r(\theta)$ for the data in Fig. 13 could be

$$C_r(\theta) = \begin{cases} 1, & \theta < \theta_1 \\ (\theta - \theta_2)/(\theta_1 - \theta_2), & \theta_1 < \theta < \theta_2 \\ 0, & \theta > \theta_2 \end{cases}.$$

Now if $p(\theta)$ is assumed to be Gaussian with a standard deviation of σ_θ, it is straightforward to calculate C_{rm}. Figure 14 shows results for stack heights of 0.25 h and 1.0 h, taking $\theta_1, \theta_2 = 14°, 22°$ and 7°, 17°, respectively. (Figure 13 includes the idealized $C_r(\theta)$ distributions.) For large variations in wind direction, the averaged concentration can clearly be greatly reduced. Knowledge of $p(\theta)$ in a given full-scale situation would allow similar estimation of the reduction in glc caused by wind meander. It should be noted that the $p(\theta)$ refers specifically to the long-time-scale variations in the mean wind direction and not to the fluctuations caused by true turbulence. A calculation of this sort therefore implicitly assumes that the two causes of fluctuations in wind direction can be separated because they occur on quite different time-scales. This may not always be the case.

5. FINAL COMMENTS AND CONCLUSIONS

For sources placed at the position corresponding to the end of the lee separation region (for $\theta = 0$), it has been shown that the terrain amplification factor, defined as the ratio of the maximum surface concentration in the presence of a hill to that in its absence, first rises and then falls with increasing source height. This is true for all wind angles in the range $0 < \theta < 45°$, and the maximum amplification occurs for source heights between 0.5 and 1.0 times the hill height. The behavior is largely independent of hill spanwise aspect ratio, although for wide hills, peak ground-level concentrations can actually be lower than in the absence of the hill if the wind angle is sufficiently large.

For a given source height, the maximum amplification factor does not necessarily occur for $\theta = 0°$; the

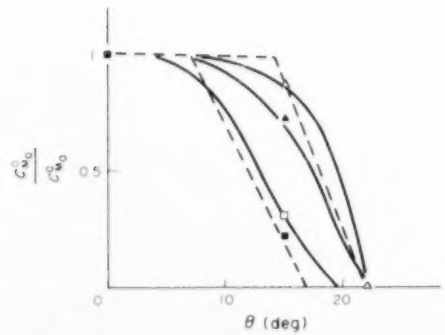

Fig. 13. Normalized concentration at P_{M0} as a function of wind direction. ———, 'ideal' distributions used for computations (see text). H_s/h: △, 0.25; ▲, 0.5; □, 0.75; ■, 1.0.

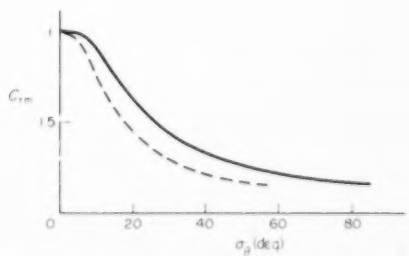

Fig. 14. Estimated reduction in surface concentration at P_{M0} caused by wind meander with standard deviation of σ_θ. H_s/h: ———, 0.25; — — —, 1.0.

results have shown that, for source heights around $H_s/h = 0.5$–0.75, A is highest for sources in the region $0.1 < y_s/W < 0.2$, i.e. at positions some 10–20% of the distance to the spanwise edge of the hill. In all cases, however, the peak glc occurs earlier than it would for flat-surface conditions, unless the wind angle is sufficiently large that the effect of the hill is negligible. For an axisymmetric hill the magnitude of the peak glc for $\theta > 0$ is always lower than the worst case at $\theta = 0$ ($H_s/h = 0.5$), whereas for a wider hill it can be a little higher than the worst case at $\theta = 0$.

Finally, for an axisymmetric hill, the ground-level concentration at the position where it is a maximum for $\theta = 0$ falls off rapidly with wind angle for all source heights. The decay is increasingly rapid as H_s/h increases but in all cases is virtually complete by $\theta = 20°$, demonstrating the sensitivity of surface-concentration levels to wind angle.

It should be emphasized that these results apply only to hills which are sufficiently steep to promote separation in the lee and for cases in which the source is located at the axial position giving maximum surface concentrations at $\theta = 0$. They therefore represent what are likely to be the worst cases in practice.

Acknowledgements—The authors wish to thank the entire staff of the EPA Fluid Modeling Facility for their cooperation during the course of the study. IPC was supported at various stages of the work by North Carolina State University as Visiting Associate Professor under EPA Agreements CR807854 and CR81'973.

REFERENCES

Arya S. P. S., Shipman M. S. and Courtney L. Y. (1981) An experimental investigation of flow and diffusion in the disturbed boundary layer over a ridge—II. Diffusion from a continuous point source. *Atmospheric Environment* **15**, 1185–1194.

Castro I. P. and Snyder W. H. (1982) A wind tunnel study of dispersion from sources downwind of three-dimensional hills. *Atmospheric Environment* **16**, 1869–1887.

Counihan J. (1975) Adiabatic atmospheric boundary layers: a review and analysis of data from the period 1880–1972. *Atmospheric Environment* **9**, 871–905.

Huber A. H., Snyder W. H., Thompson R. S. and Lawson R. E., Jr (1976) Stack placement in the lee of a mountain ridge: a wind tunnel study. Rep. No. EPA-600/4-76-047. E.P.A., Research Triangle Park, NC, 45 pp.

Khurshudyan L. H., Snyder W. H. and Nekrasov I. V. (1981) Flow and dispersion of pollutants over two-dimensional hills: summary report on joint Soviet–American study. Rep. No. EPA-600/4-81-067. E.P.A., Research Triangle Park, NC, 143 pp.

Pasquill F. (1974) *Atmospheric Diffusion*, 429 pp., 2nd edn. Ellis Horwood, Chichester; John Wiley, New York.

Robins A. G. (1978) Plume dispersion from ground-level sources in simulated atmospheric boundary layers. *Atmospheric Environment* **12**, 1033–1044.

Snyder W. H. and Britter R. E. (1987) A wind tunnel study of the flow structure and dispersion from sources upwind of three-dimensional hills. *Atmospheric Environment* **21**, 735–751.

Turner D. B. (1970) Workbook of atmospheric dispersion estimates. Office of Air Programs Publ. No. AP-26. E.P.A., Research Triangle Park, NC.

NOTICE

This document has been reviewed in accordance with U.S. Environmental Protection Agency policy and approved for publication. Mention of trade names or commercial products does not constitute endorsement or recommendation for use.

This article documents research that was conducted under the auspices of the U.S. Environmental Protection Agency (USEPA). As an arm of the government, the USEPA has a paid up, non-exclusive, irrevocable, worldwide license to reproduce, prepare derivative works, and distribute to the public all of the material contained herein, and to grant others acting on its behalf the right to do so. The USEPA grants to the National Technical Information Service, Department of Commerce, the right to act as its agent in the distribution of this material.